ADVANCED ENERGY MATERIALS

# Supporting Information

for *Adv. Energy Mater.,* DOI: 10.1002/aenm.202203325

# Weak Electron–Phonon Coupling and Enhanced Thermoelectric Performance in n-type PbTe–$Cu_2Se$ via Dynamic Phase Conversion

*Ming Wu, Hong-Hua Cui, Songting Cai, Shiqiang Hao, Yukun Liu, Trevor P. Bailey, Yinying Zhang, Zixuan Chen, Yubo Luo, Ctirad Uher, Christopher Wolverton, Vinayak P. Dravid, Yan Yu, Zhong-Zhen Luo,* Zhigang Zou, Qingyu Yan,* and Mercouri G. Kanatzidis**

# Supporting Information

# Weak electron−phonon coupling and enhanced thermoelectric performance in n-type PbTe−$Cu_2Se$ via dynamic phase conversion

Ming Wu,[1,10] Hong-Hua Cui,[2,10] Songting Cai,[3,4] Shiqiang Hao,[4] Yukun Liu,[4] Trevor P. Bailey,[5] Yinying Zhang,[5] Zixuan Chen,[1] Yubo Luo,[6] Ctirad Uher,[5] Christopher Wolverton,[4] Vinayak P. Dravid,[4] Yan Yu,[1,7,9] Zhong-Zhen Luo,[1,3,7,8,*] Zhigang Zou,[1,7,9] Qingyu Yan,[8,*] Mercouri G. Kanatzidis[3,*]

[1]Key Laboratory of Eco-materials Advanced Technology, College of Materials Science and Engineering, Fuzhou University, Fuzhou, 350108, China

[2]Mechanical and Electrical Engineering Practice Center, Fuzhou University, Fuzhou, 350108, China

[3]Department of Chemistry, Northwestern University, Evanston, Illinois 60208, United States

[4]Department of Materials Science and Engineering, Northwestern University, Evanston, Illinois 60208, United States

[5]Department of Physics, University of Michigan, Ann Arbor, Michigan 48109, United States

[6]State Key Laboratory of Materials Processing and Die & Mould Technology, School of Materials Science and Engineering, Huazhong University of Science and Technology, Wuhan 430074, P. R. China

[7]Fujian Science & Technology Innovation Laboratory for Optoelectronic Information of China, Fuzhou, Fujian 350108, P. R. China

[8]School of Materials Science and Engineering, Nanyang Technological University, 50 Nanyang Avenue 639798, Singapore

[9]Eco-materials and Renewable Energy Research Center, College of Engineering and Applied Sciences, Nanjing University, Nanjing, 210093, China

[10]These authors contributed equally: Ming Wu, Hong-Hua Cui

**Spark Plasma Sintering (SPS).** The obtained ingots of $Pb_{0.975}Ga_{0.025}Te$-x%$Cu_2Se$ were hand-ground into fine powders and subsequently densified using the SPS technique (SPS-211LX, Fuji Electronic Industrial Co. Ltd.) in a 12.7 mm diameter graphite die. The sintering temperature and uniaxial pressures are 823 K and 40 MPa, respectively. The disk-shaped pellets showed 96% or higher relative mass densities with a thickness of ~10 mm (Table S1, Supporting Information).

**Powder X-ray Diffraction (PXRD) Characterization.** The room temperature PXRD patterns measurement (Rigaku Miniflex powder X-ray diffractometer with Cu $K_\alpha$ $\lambda$ = 1.5418 Å) were collected in the range of 2$\theta$ from 20−80° with the scan increment of 0.02°.

**In-situ PXRD Characterization.** The In-situ PXRD patterns of $Pb_{0.975}Ga_{0.025}Te$-3%$Cu_2Se$ from 303 K to 823 K were performed on D8 ADVANCE (Bruker) with a voltage of 40 kV and current of 40 mA. The divergence and scattering slits are 3 and 5 mm, respectively.

**Electronic Transport Properties.** The rectangular shape bars (~11 mm × 4 mm × 4 mm), cut and polished from SPSed pellets, were used for the simultaneous electrical conductivity and Seebeck coefficient measurements. The test was performed on a commercial Ulvac Riko ZEM-3 system under a low-pressure helium atmosphere from 300 K to 873 K. The uncertainty of the measure is estimated to be ~5%.

**X-ray photoelectron spectroscopy (XPS) measurements.** XPS spectra were tested on a Thermo Scientific ESCALAB 250 Xi spectrometer with a monochromatic Al Kα X-ray source (1486.6 eV) under an ultrahigh vacuum (< $10^{-8}$ mbar). The pass energies for the survey and high-resolution scans are 150 eV and 25 eV, respectively. The spectra were calibrated with the C 1s peak binding energy at 284.7 eV (carbon tape).

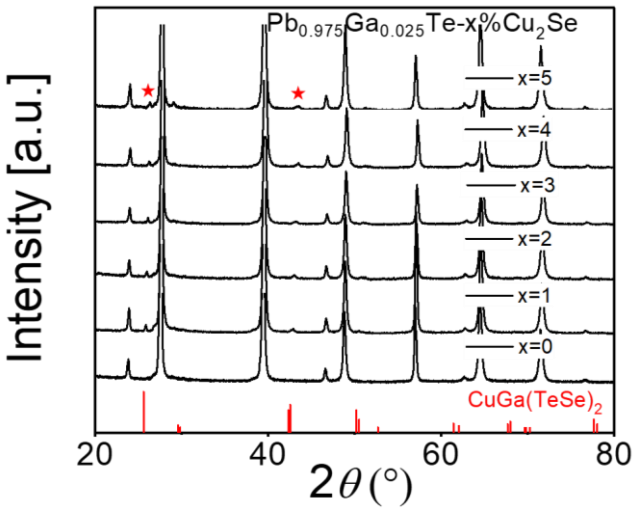


**Figure S1.** The zoomed-in view of PXRD patterns of $Pb_{0.975}Ga_{0.025}Te$-x%$Cu_2Se$ (x = 0, 1, 2, 3, 4, and 5) at room temperature, revealing that a trace amount of $CuGa(Te,Se)_2$ phase can be detected.

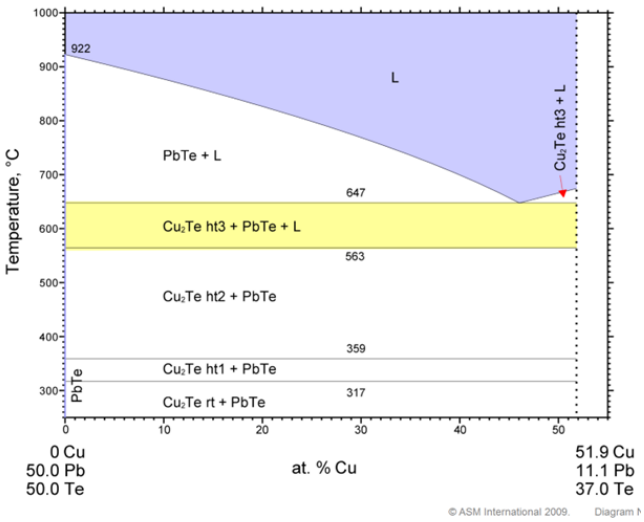


**Figure S2**. The phase diagram of the PbTe-$Cu_2Te$ system. Below 650 °C the solid solubility of Cu in PbTe is very low. (Grytsiv V.I., and Vengel' P.F., PbTe-Cu and PbTe-Cu2Te polythermal cross sections of the Pb-Te-Cu ternary system, *Inorg. Mater.*, 20, **1984**, 1713-1716)

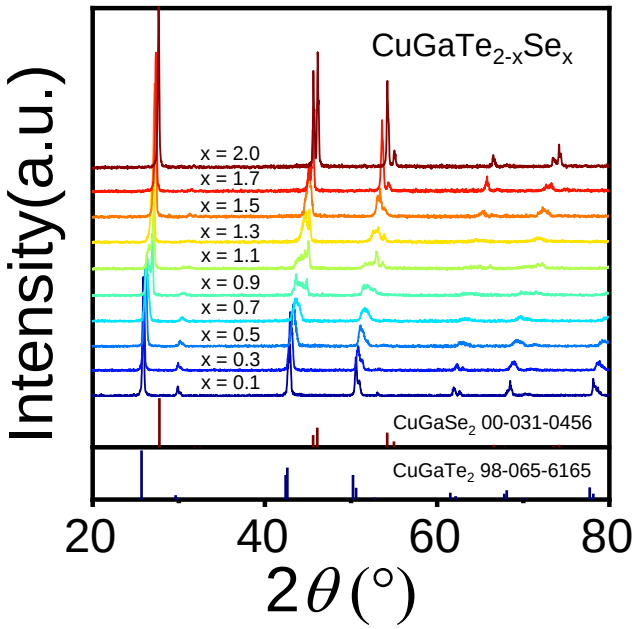


**Figure S3.** The PXRD patterns of $CuGaTe_{1-x}Se_x$ phase (x = 0.1, 0.3, 0.5, 0.7, 0.9, 1.1, 1.3, 1.5, 1.7, and 2.0).

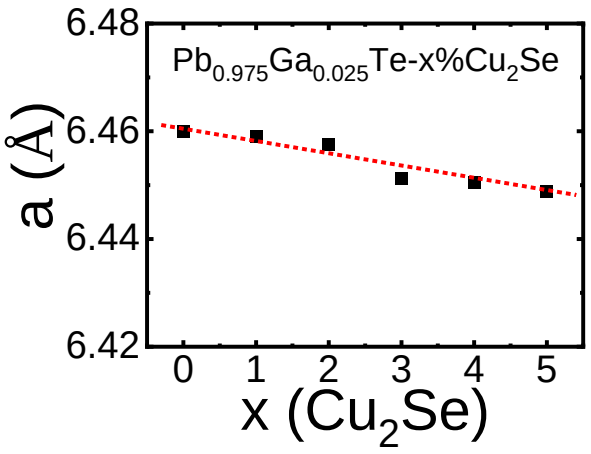


**Figure S4.** Refined lattice parameters of $Pb_{0.975}Ga_{0.025}Te$-x%$Cu_2Se$ (x = 0, 1, 2, 3, 4, and 5). The red dashed line is a guide to the eye.

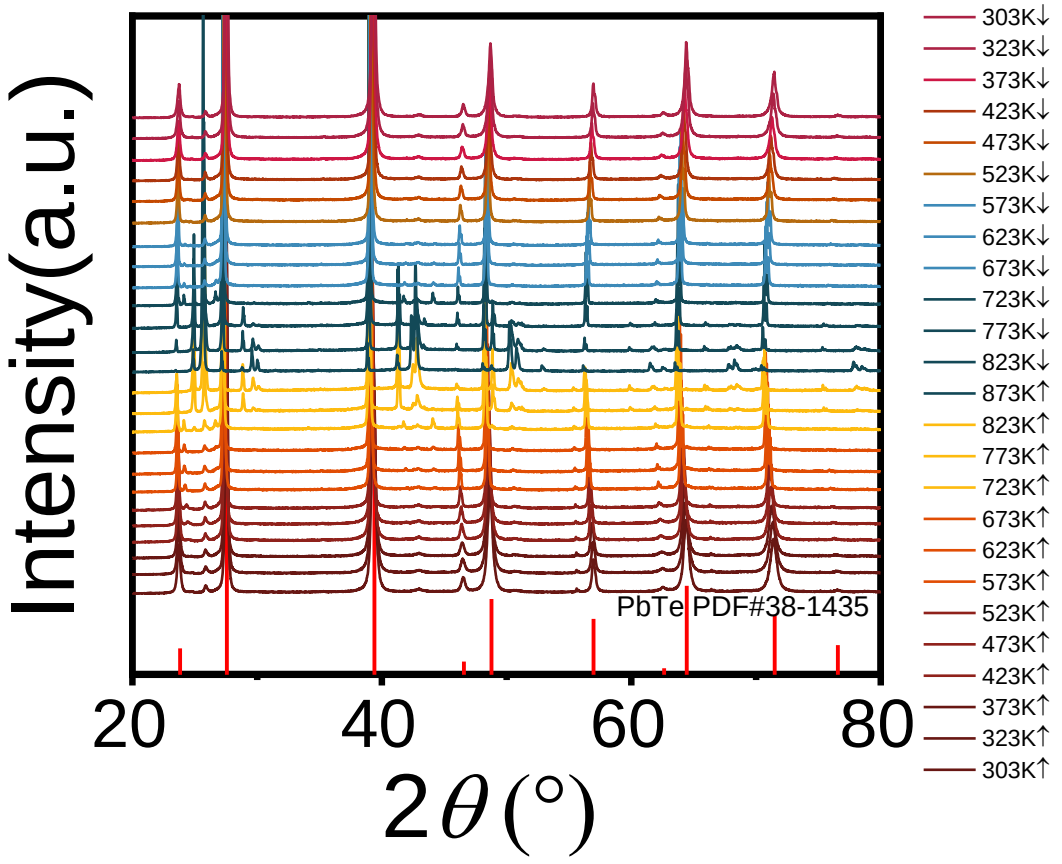


**Figure S5.** In-situ PXRD patterns of $Pb_{0.975}Ga_{0.025}Te$-3%$Cu_2Se$ sample from 303 K to 873 K and 873 K to 303 K. The XRD patterns at the heating and cooling processes indicated the stability of the sample and the dynamic phase conversion.

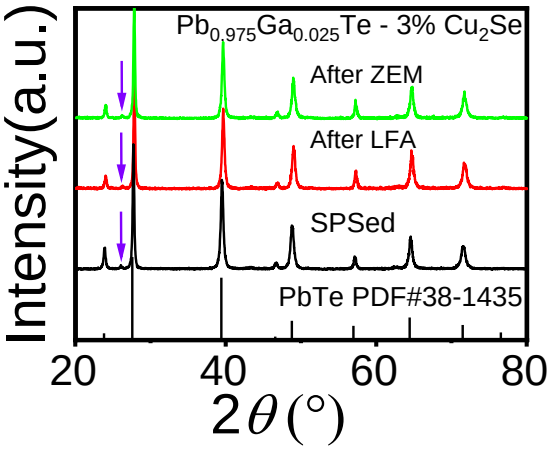


**Figure S6.** The PXRD patterns of $Pb_{0.975}Ga_{0.025}Te$-3%$Cu_2Se$ before (SPSed) and after thermoelectrical measurements (after LFA and ZEM) reveal the excellent stability of the compound.

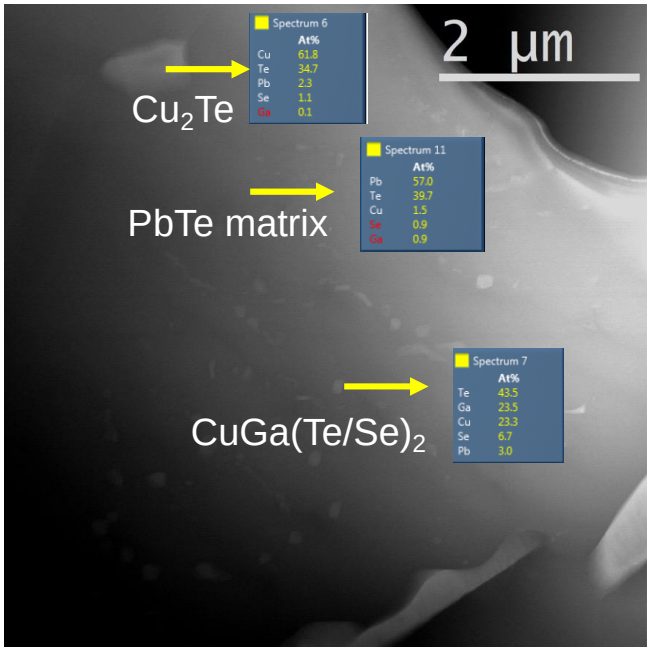


**Figure S7.** HAADF image of $Pb_{0.975}Ga_{0.025}Te$-3%$Cu_2Se$ with quantitative EDS results in three typical regions (PbTe matrix, $CuGa(Te/Se)_2$, and $Cu_2Te$).

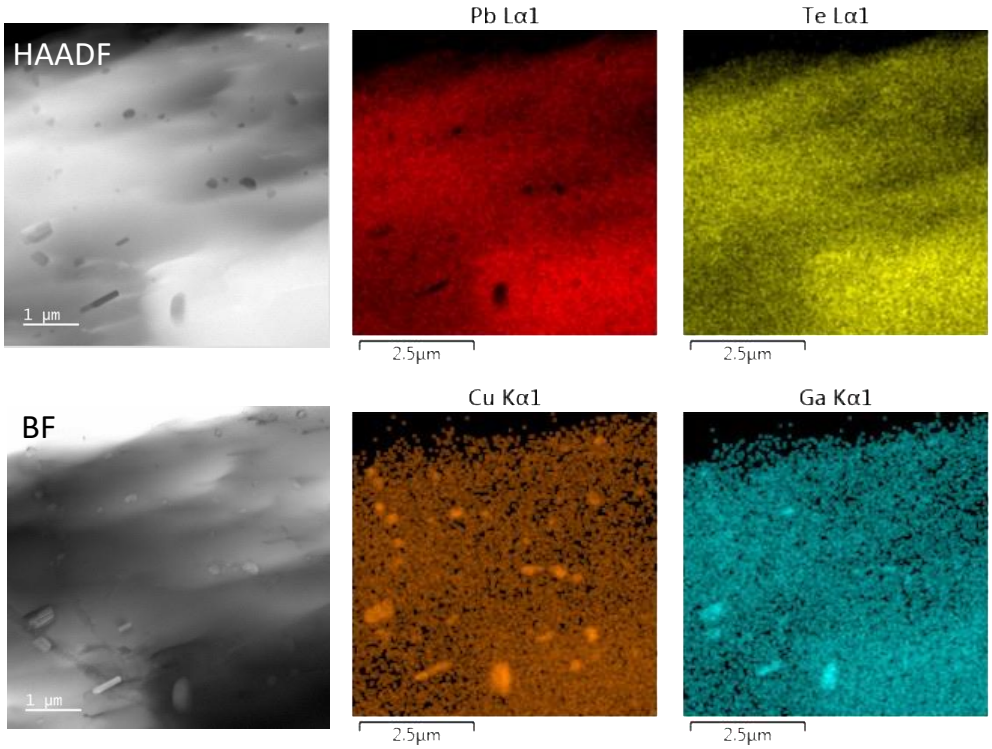


**Figure S8.** HAADF, BF image of the $Pb_{0.975}Ga_{0.025}Te$-3%$Cu_2Se$ sample after thermoelectrical measurements and its corresponding EDS mappings.

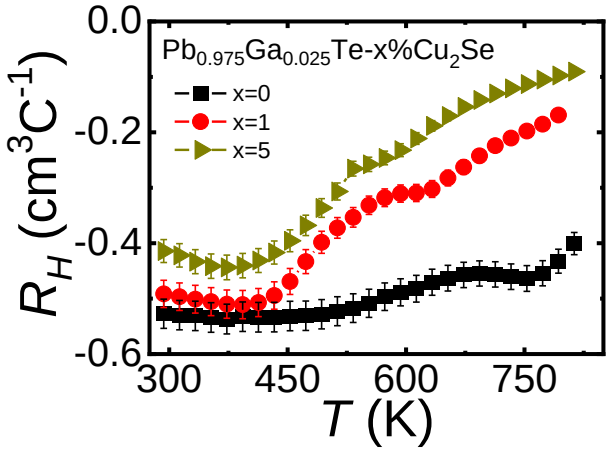


**Figure S9.** Temperature-dependent $R_H$ for $Pb_{0.975}Ga_{0.025}Te$-x%$Cu_2Se$ (x = 0, 1, and 5).

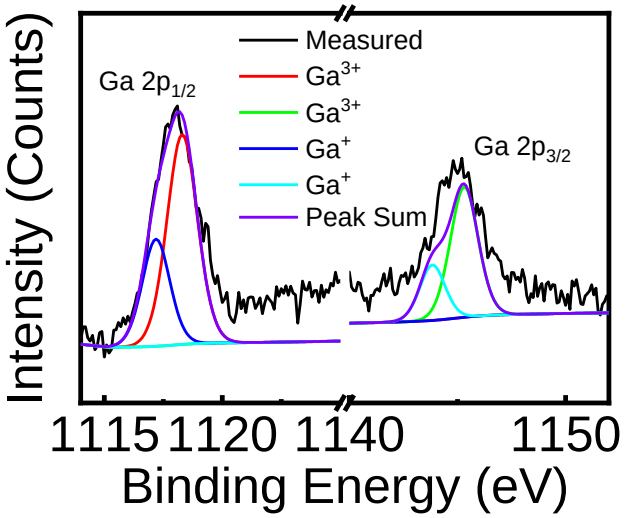


**Figure S10**. The X-ray photoelectron spectra (XPS) of Ga $2p^{1/2}$ and $2p^{3/2}$ core states for $Ga^{3+}$ and $Ga^{+}$ states in $Pb_{0.975}Ga_{0.025}Te$-5%$Cu_2Se$.

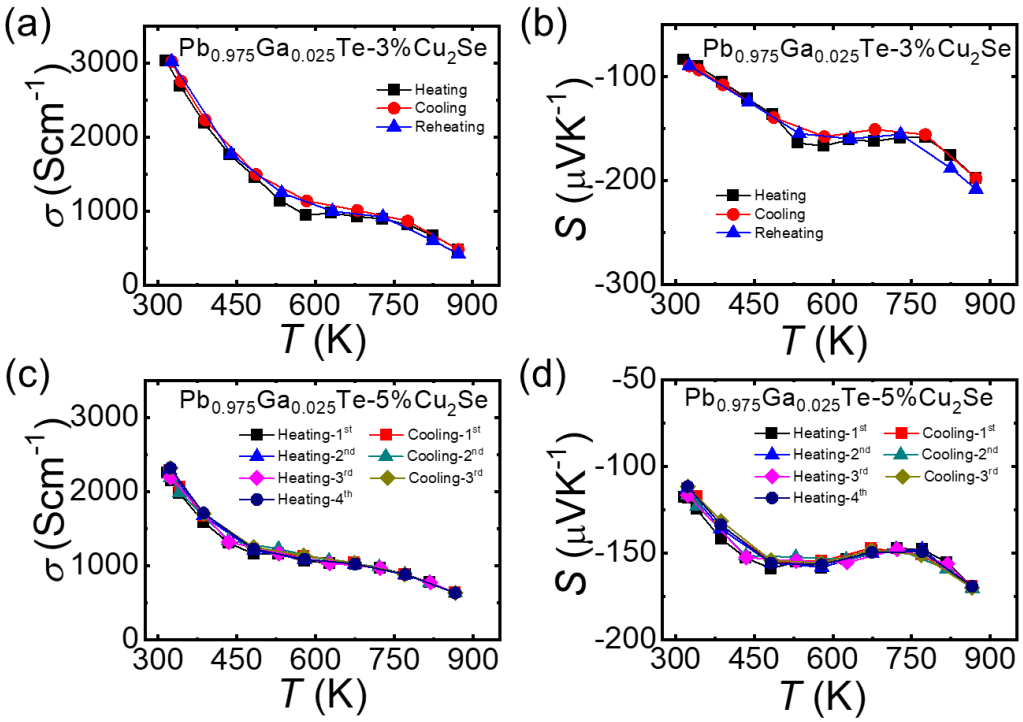


**Figure S12**. The electrical conductivity and Seebeck coefficient for $Pb_{0.975}Ga_{0.025}Te$-x%$Cu_2Se$ (x = 3 and 5) are stable under thermal cycling with heating-cooling-repeated measurements, showing good repeatability.

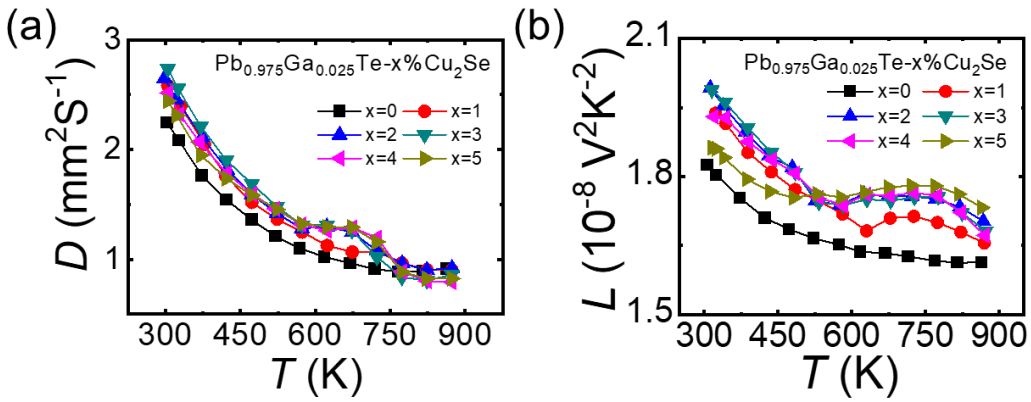


**Figure S12**. Temperature-dependent (a) thermal diffusivity, *D* and (d) Lorenz numbers, *L* of $Pb_{0.975}Ga_{0.025}Te$-x%$Cu_2Se$ (x = 0, 1, 2, 3, 4, and 5).

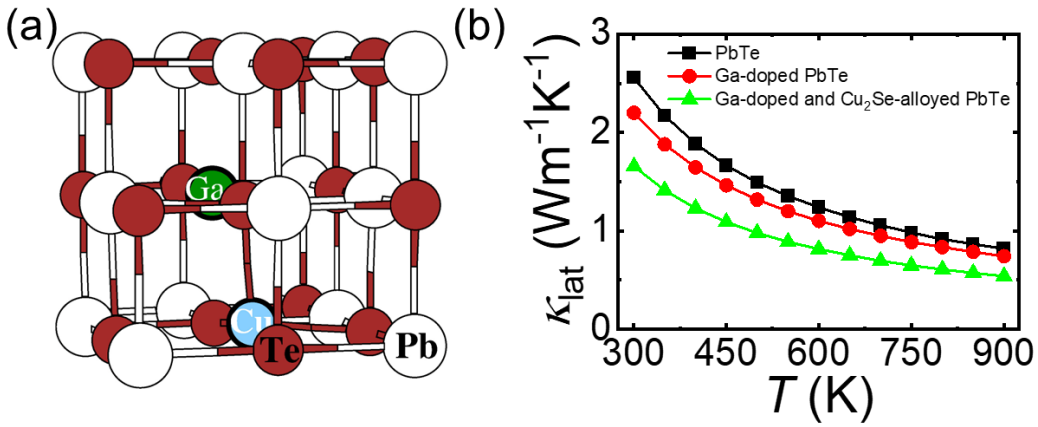


**Figure S13**. (a) Illustration of the Ga-doped and $Cu_2Se$ alloyed PbTe structure model with the Cu-Ga-Se complex and (b) Comparison of the calculated $\kappa_{lat}$ from the DFT phonon dispersion for pure PbTe, Ga-doped PbTe, and Ga-doped and $Cu_2Se$ alloyed PbTe as a function of temperature.

**Table S1.** Mass densities for $Pb_{0.975}Ga_{0.025}Te$-x%$Cu_2Se$ (x = 0, 1, 2, 3, 4, and 5) at room temperature.

| Composition | Measured density, $gcm^{-3}$ | Theoretical density, % |
|---|---|---|
| $Pb_{0.975}Ga_{0.025}Te$ | 7.94 | 97.4 |
| $Pb_{0.975}Ga_{0.025}Te$-1%$Cu_2Se$ | 7.85 | 96.5 |
| $Pb_{0.975}Ga_{0.025}Te$-2%$Cu_2Se$ | 7.88 | 97.0 |
| $Pb_{0.975}Ga_{0.025}Te$-3%$Cu_2Se$ | 7.83 | 96.5 |
| $Pb_{0.975}Ga_{0.025}Te$-4%$Cu_2Se$ | 7.80 | 96.4 |
| $Pb_{0.975}Ga_{0.025}Te$-5%$Cu_2Se$ | 7.85 | 97.1 |